Dependence on beam energy and nuclear equation of state of anisotropic flow and particle production in low-energy heavy-ion collisions

Sumit Kumar Kundu [1], Yoshini Bailung [1], Sudhir Pandurang Rode [1,*], Partha Pratim Bhaduri,[2] and Ankhi Roy [1]

[1]*Department of Physics, School of Basic Sciences, Indian Institute of Technology Indore, Indore 453552 India*
[2]*Variable Energy Cyclotron Centre, HBNI, 1/AF Bidhan Nagar, Kolkata 700064, India*

We analyze various flow coefficients of anisotropic momentum distribution of final state particles in mid-central ($b = 5$–9 fm) Au + Au collisions in the beam energy range $E_{Lab} = 1A$–$158A$ GeV. Different variants of the ultrarelativistic quantum molecular dynamics (UrQMD) model, namely the pure transport (cascade) mode and the hybrid mode, are employed for this investigation. In the hybrid UrQMD model, the ideal hydrodynamical evolution is integrated with the pure transport calculation for description of the evolution of the fireball. We opt for the different available equations of state (EoS) replicating the hadronic as well as partonic degrees of freedom together with possible phase transitions, viz., hadron gas, chiral + deconfinement EoS, and bag model EoS, to investigate their effect on the properties of the final state particles. We also attempt to gain insights about the dynamics of the medium by studying different features of particle production such as particle ratios and net-proton rapidity distribution. The results and conclusions drawn here would be useful to understand the response of various observables to the underlying physics of the model as well as to make comparisons with the upcoming measurements of the future experiments at the Facility for Antiproton and Ion Research (FAIR) and the Nuclotron-based Ion Collider fAcility (NICA).

I. INTRODUCTION

One of the main objectives of modern day relativistic heavy-ion physics research is to understand the phase structure of strongly interacting matter at extreme conditions of temperatures and net baryon densities in the laboratory [1,2]. The possible existence of a critical point of QCD matter along with a phase transition to deconfined state motivates the high energy community to continue the efforts in this direction. Exploration of QCD matter at finite baryon densities is relatively less extensive compared to that created at negligible baryon densities. An ample number of investigations have been performed in the latter direction in the past two decades with various experiments at the Relativistic Heavy Ion Collider (RHIC) [3,4] and the Large Hadron Collider (LHC) [5–7]. Upcoming experiments at future accelerator facilities such as the Nuclotron-based Ion Collider fAcility (NICA) [8] and the Facility for Antiproton and Ion Research (FAIR) [9,10] aim to probe baryon rich matter with good precision. However an optimal use of these facilities demands an extensive analysis of the available data and model based studies of different observables in a similar energy domain.

The anisotropic flow of the particles emitted in noncentral relativistic heavy-ion collisions is considered a promising observable to investigate the collective effects of the produced medium. Originating due to the pressure gradient as a result of the multiple scatterings among the constituents of the medium, it is vulnerable to the underlying nuclear equation of state. Azimuthal anisotropy in momentum distribution of the final state particles is quantified in terms of various harmonic coefficients using Fourier series. These different anisotropic flow coefficients can be expressed as

$$v_n = \langle \cos[n(\phi - \Psi)] \rangle$$

where the azimuthal angle of the particle and the reaction plane angle are indicated by ϕ and Ψ, respectively. Moreover, v_n is defined as directed flow (v_1), elliptic flow (v_2), triangular flow (v_3), quadrangular flow (v_4) for $n = 1, 2, 3, 4$ and so on, respectively. These coefficients are believed to provide insight into the dynamics of the fireball. For instance, significant magnitude of v_2 has shed light on the possibility that the bulk of the produced matter achieves conditions close to local thermal equilibrium. The pressure gradient developed due to rescatterings in the early stage of collisions converts the initial state spatial anisotropy to final state momentum anisotropy and v_2. Several experiments [11,12] at different energies have examined v_2 for the possible signature of thermalization of the produced medium. A substantial amount of study has been performed to inspect v_2 in low energy collisions at various beam energy ranges [13–15], availing a variety of microscopic transport models [16–19]. At low beam energies, change of sign, i.e., transition from out-of-plane to in-plane flow, has been observed [20,21].

On the other hand, the directed flow, v_1, quantifies the deflection of the produced particles in the reaction plane. Sensitivity to the longitudinal dynamics and possibility of being developed prior to v_2 [22–24] make v_1 worth studying in

*sudhirrode11@gmail.com

relativistic nuclear collisions. The magnitude of v_1 is expected to vanish in the vicinity of the phase transition due to softening of the underlying EoS and this makes it an exciting observable for analysis at RHIC-BES, FAIR, and NICA energies. A plethora of the activities have been carried out in this direction in a past few decades in various experiments. For instance, the slope of v_1, being the measure of the signal strength, shows linearity at the midrapidity at Alternating Gradient Synchrotron (AGS) [25–27] energies and below. However, this linearity at midrapidity is not expected to be maintained at higher beam energies because the slope at midrapidity is found to be different than that at beam rapidity at energies above those available at the Super Proton Synchrotron (SPS) [28–30]. Hydrodynamical model calculations indicate that the so-called structure "wiggle" is sensitive to the underlying EoS [31–33]. Study of higher order harmonics has gained some attention in the past few years and is expected to provide further insights about the produced fireball. The fourth-order harmonic coefficient, v_4, has been known to be sensitive to intrinsic v_2 [34–36] and therefore it is quite interesting to investigate it over a wider range of beam energies, which has also been attempted using the jet AA microscopic transport model JAM [23,37]. It bears some crucial details about the collision dynamics predicted by hydrodynamical calculations [36].

In this article, we make some efforts to address the nuclear equation-of-state dependence of the anisotropic flow coefficients and particle production in noncentral ($b = 5$–9 fm) Au-Au collisions in very wide ranges of the beam energies, $E_{\text{Lab}} = 1A$–$158A$ GeV, which span existing GSI-SIS energy of the HADES experiment up to the top SPS energy. It is found that the corresponding $\langle N_{\text{part}} \rangle$ values in the chosen impact parameter range $b = 5$–9 fm cover approximately 10–40% centrality class [38]. For our study, we employ the publicly available version 3.4 of the ultrarelativistic quantum molecular dynamics (UrQMD) model with different configurations of hybrid model for the intermediate hydrodynamical stage, viz., hadron gas (HG), chiral + deconfinement EoS, and bag model EoS, along with the pure transport approach. The latter two hybrid versions mimic the partonic degrees of freedom and phase transition in the medium; however, the first one includes hadronic degrees of freedom only. The reaction plane angle (Ψ) is taken to be zero within this model. It is important to note that the present study is not a pioneering attempt to apply a hybrid UrQMD model to study collective flow excitations at these beam energies. In Ref. [39], the authors have calculated the transverse momentum and rapidity dependence of v_1 and v_2 at $40A$ and $160A$ GeV in Pb + Pb collisions using the standard UrQMD model at various centralities, which showed disagreement with experimental measurements by the NA49 Collaboration. In addition, v_1 and v_2 were also studied as a function of beam energy in the range of $E_{\text{Lab}} = 90A$ MeV to $E_{\text{cm}} = 200A$ GeV, and also showed disagreement with the available data. In Ref. [40], the excitation function of v_2 was examined in the range of GSI-SIS to CERN-SPS energies using UrQMD with the HG EoS within a hybrid approach, and other harmonics such as v_2 and v_3 were studied with a chiral EoS in Au-Au systems between $\sqrt{s_{NN}} = 5$ and 200 GeV [15]. The collision energy dependence of v_1 was tested using the

hybrid model for nuclear reactions between $\sqrt{s_{NN}} = 3$ and 20 GeV [41]. In our previous work [42], study of nuclear equation-of-state dependence of anisotropic flow was performed using a hybrid UrQMD model within $6A$–$25A$ GeV with HG and chiral EoS. All these results seem to suggest that the quantitative applicability of this model a to real scenario has some limitations. However, in this paper, we qualitatively aim to understand the effect of various nuclear equations of state on the flow harmonics and hence gain some insights about the dynamics leading to their development at various beam energies ranging from $1A$ to $158A$ GeV.

Besides anisotropic flow, we also attempt to study the EoS dependence of particle production in noncentral collisions. The particle ratios of various species are examined for this purpose. We also look at the net-proton rapidity distributions. The structure of the net-proton rapidity spectra at midrapidity is expected to be sensitive to the underlying EoS of the nuclear fireball. In central collisions, adequate studies have been performed in this direction. In Refs. [43–47], the authors have quantified the structure of net proton rapidity distribution at midrapidity in central collisions, in terms of reduced curvature. It was studied as a function of beam energy and compared with predictions incorporating various possible scenarios of fireball expansion. In the present article we extend these studies to mid-central collisions.

This article is arranged in the following order. In Sec. II, basic principles of the UrQMD model and its different variants are briefly introduced. The obtained results on anisotropic flow coefficients and particle production properties over a very wide range of colliding energies are presented in Sec. III. Finally we summarize the results in Sec. IV.

II. MODEL DESCRIPTION

For a detailed description of the ultrarelativistic quantum molecular dynamics (UrQMD) model, the reader is referred to Refs. [16,17,48]. The purpose of the UrQMD model is to simulate high energy nucleus-nucleus collisions. The initializations of the target and projectile nuclei in coordinate and momentum space are done with the help of a Woods-Saxon profile and the Fermi gas model, respectively. Together with the various experimental inputs such as cross sections and decay widths, the collisions in the model are described in terms of interactions among resonances, hadrons, and their excited states at low energies and in terms of excitations of color strings with their subsequent fragmentation into hadrons at higher energies [17]. The propagation of hadrons takes place on straight line trajectories amid subsequent collisions.

In the hybrid version of UrQMD, the ideal $(3 + 1)$d relativistic fluid dynamical evolution using SHASTA algorithm [49,50] is combined with the pure transport approach for a better modeling of the intermediate hot and dense stages of the collision. The calculation of the initial state of the hydrodynamical evolution is crucial to account for the nonequilibrium nature of the early stage; moreover, this also incorporates event-by-event fluctuations of the initial states. The hydrodynamical evolution commences upon crossing of the two Lorentz-contracted nuclei [48]. This choice of the initial time ensures that all initial baryon-baryon scatterings and
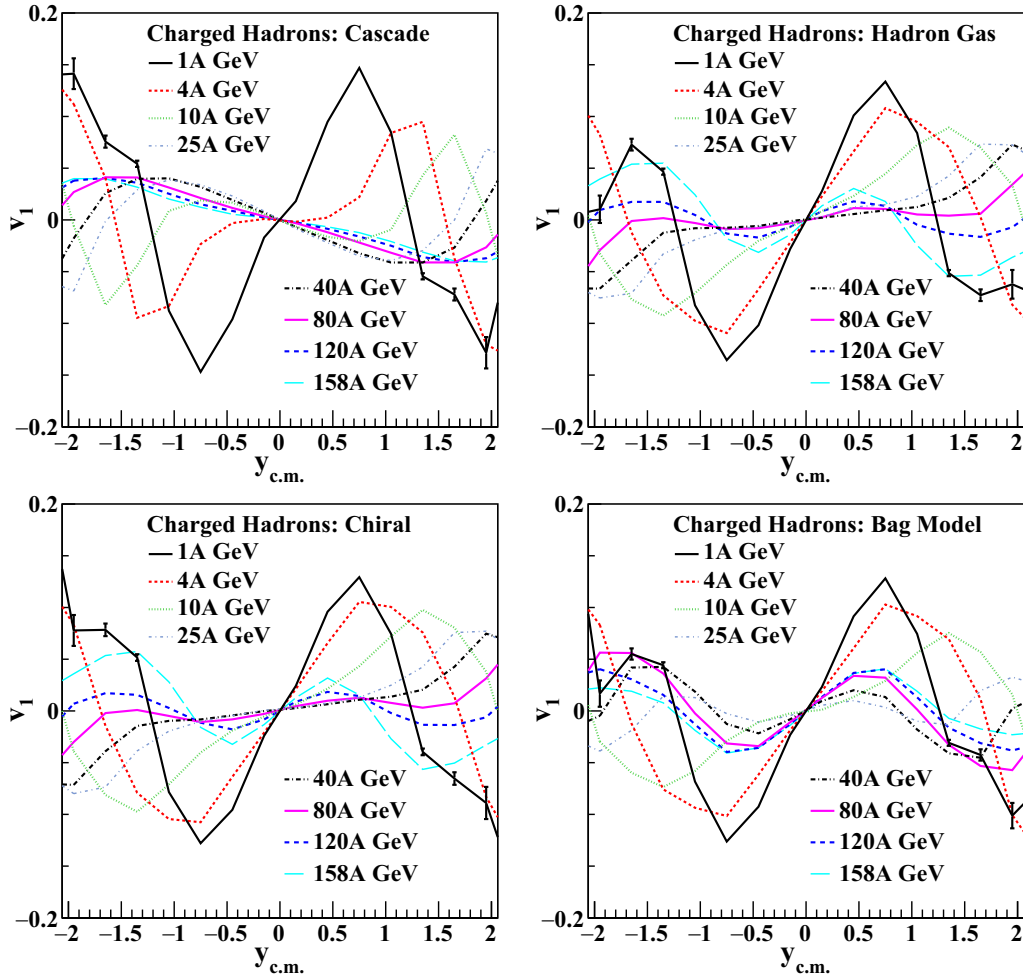
FIG. 1. Directed flow of charged hadrons as a function of rapidity at different beam energies for different configurations of UrQMD for noncentral ($b = 5$–9 fm corresponds to approximately 10-40% central) Au-Au collisions.

consequent energy deposition have taken place, and represents the lower limit of the timescale for thermalization. Thereafter, the mapping of particles, which are treated as "pointlike" in the initial stage, to the hydrodynamic grid is performed while the spectators are propagated in the cascade. This is immediately followed by the hydrodynamical evolution, for which the equation of state (EoS) serves as one of the important inputs. After the local energy density ϵ drops below five times the ground state energy density ϵ_0 [48], the hydrodynamical evolution ceases and the hadronization is performed by mapping the hydrodynamical fields to the hadrons using the Cooper-Frye prescription [51]. The model offers two different freeze-out criteria [52]. In the isochronous freeze-out (IF) scenario, all hydrodynamic cells are mapped onto particles at the same time, provided the energy density drops below the critical value in all cells. Alternatively, in the gradual freeze-out (GF) scenario, 0.2 fm thick transverse slices are particlized when energy density in all cells of each individual slice drops below the critical value. Employment of gradual transition leads to a rapidity independent transition temperature without artificial time dilation effects. In our calculations we use the GF scenario [53]. The authors of Ref. [54] have seen that such freeze-out conditions provide the best de-

scription of the data for the mean transverse mass excitation function. Thereafter, the hadrons are evolved through rescatterings and decays until the decoupling of the system.

In hydro mode, there are several available EoS that can be employed. One of them is the hadron gas (HG) EoS [55], which has underlying degrees of freedom similar to the pure transport approach. It consists of a noninteracting gas of hadrons described by a grand canonical ensemble and does not incorporate any type of phase transition. This gives an excellent opportunity to compare the hydrodynamical and pure transport approaches on equal footing.

The other possible choice includes the bag model EoS [50]. It has an inbuilt first-order deconfinement phase transition anticipated at finite baryon densities. In this EoS, an improved version of the σ-ω model with realistic effective nucleon mass and ground state incompressibility values is employed in the case of hadronic matter, whereas the standard MIT bag model [56] is recruited for the QGP phase. During the transition, both these phases are matched with the help of Gibbs' conditions for phase equilibrium [50].

Moving on, there is another available EoS named the chiral + deconfinement EoS [57] employed in this investigation. Both chiral as well as deconfinement phase transitions are
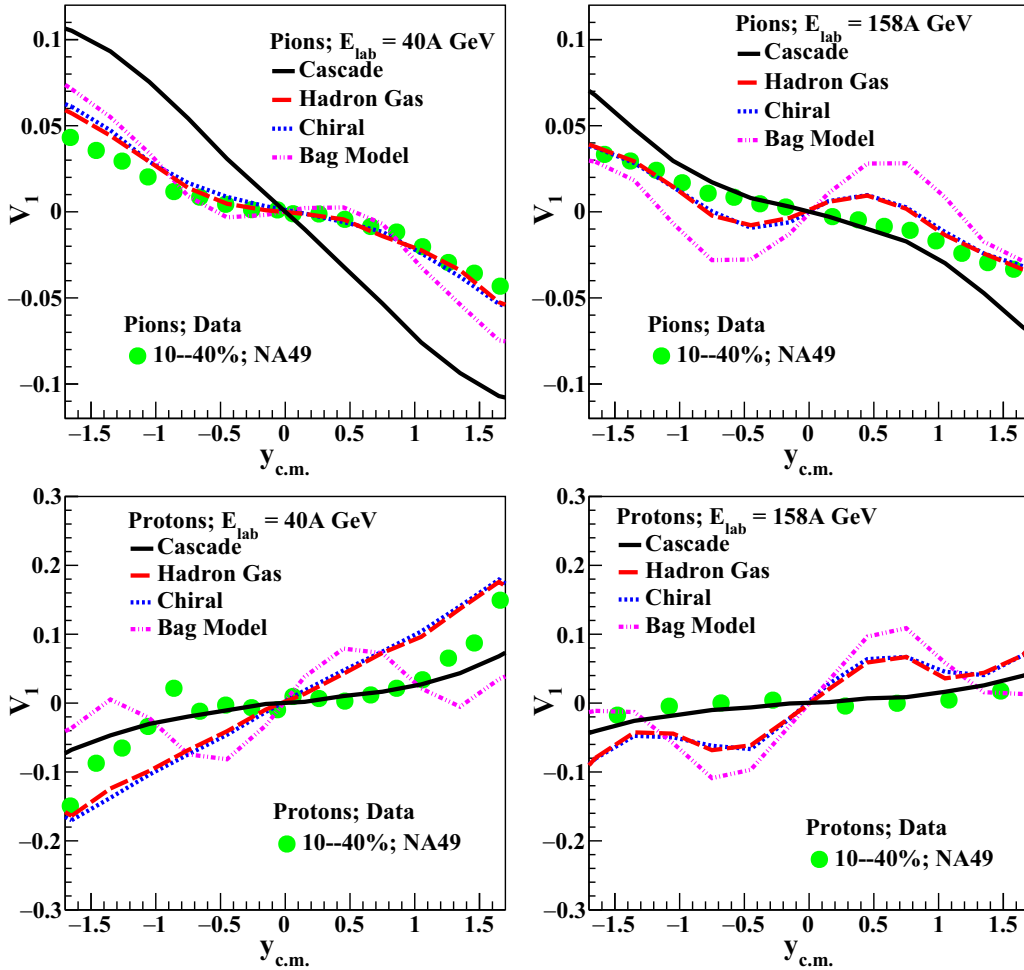
FIG. 2. Comparison of directed flow of pions and protons as a function of rapidity for different configurations of UrQMD with measured directed flow for $p_T < 2\,\mathrm{GeV}/c$ for noncentral ($b = 5$–$9\,\mathrm{fm}$ corresponds to approximately 10-40% central) Au-Au collisions with NA49 experimental measurements [58] at $40A$ and $158A$ GeV in Pb-Pb collisions.

included in this EoS, while the latter is a continuous cross over for all finite net baryon densities (μ_B). The chiral phase transition is administrated by hadronic interactions whereas the deconfinement transition occurs via quarks and the Polyakov potential. The partonic degrees of freedom only show up at higher temperatures where hadrons disappear. At vanishing μ_B this EoS matches well with the lattice QCD simulations. Independent use of three different EoS within the hybrid UrQMD model enables us to compare three distinct fireball evolution scenarios over the entire energy domain investigated in this work.

III. RESULTS AND DISCUSSION

In this section, we present the results of our investigations on various anisotropic flow coefficients at different beam energies for charged and identified hadrons. All the three EoS mentioned above are employed for this purpose. Then we move on to investigate the sensitivity of underlying EoS to the different particle production mechanisms such as strange to nonstrange ratio, baryon to meson ratio, and so on. Finally, we also look at the net proton rapidity spectra for different EoS

to look for possible insights into the longitudinal dynamics of the medium.

A. Anisotropic flow coefficients

Among various harmonic coefficients, v_1 is believed to be sensitive to the longitudinal dynamics of the QCD medium. Therefore, we start by estimating the v_1 of charged hadrons as a function of rapidity at different beam energies and for pure transport and hybrid versions of the UrQMD model. The results are shown in Fig. 1. In the presence of hydrodynamic expansion, the slope at midrapidity remains positive at all investigated energies. For a pure transport approach, the slope initially remains positive and eventually becomes negative.

Directed flows of pions and protons for $p_T < 2\,\mathrm{GeV}/c$ at $40A$ and $158A$ GeV are compared with the existing measurement by the NA49 experiment [58] at SPS in 10–40% central Au $+$ Au collisions as shown in Fig. 2. hybrid modes fails to explain the slope of v_1 except for pions at $40A$ GeV. The pure transport approach is seen to do a better job of explaining the proton v_1 reasonably well at both energies at midrapidity, an observation in line with previous studies [39,59].
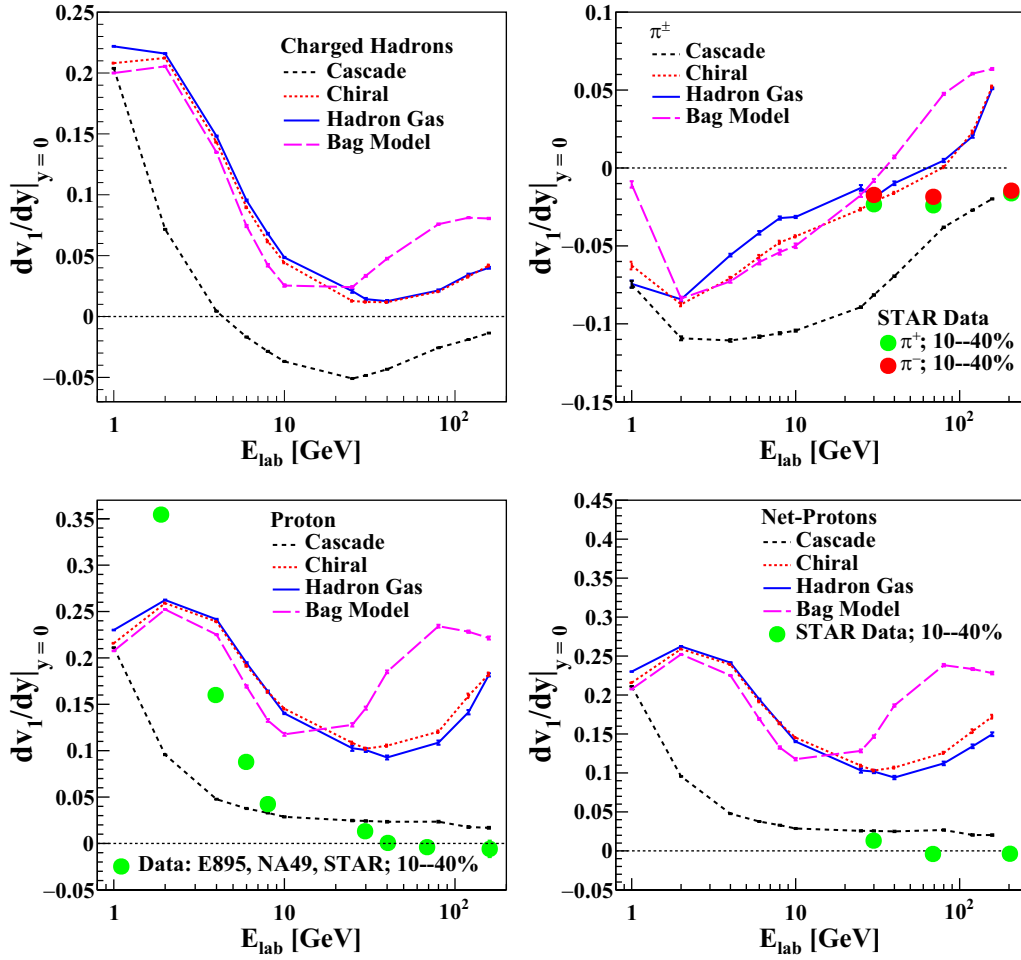
FIG. 3. Slope of the directed flow of charged hadrons, pions, protons, and net protons as a function of beam energy at midrapidity for different configurations of UrQMD for noncentral ($b = 5$–9 fm corresponds to approximately 10-40% central) Au-Au collisions with E895 [25] and STAR [61] experimental measurements in Au-Au collisions and with NA49 [58] experimental measurements in Pb-Pb collisions.

Slopes of directed flows of charged hadrons, pions, protons, and net protons as a function of beam energy are quantified in Fig. 3. The slope is obtained by fitting differential directed flow [$v_1(y)$] using first-order polynomial at midrapidity. Similar values of slopes are noticed in all three cases of hydro mode up to 10A GeV for all species. The slope using cascade mode is smaller compared to hydro mode. For pions, the slope obtained in cascade mode always remain negative at all investigated energies and shows transition from negative to positive value between 30A to 80A GeV once hydrodynamic expansion is switched on. The slope does not show any sensitivity to underlying degress of freedom brought by HG and chiral EoS in the charged hadrons case, which was also observed in our previous study between beam energies 6A and 25A GeV [42]. Moreover, we tend to see a slight hint of sensitivity in the case of protons and net protons beyond 25A GeV; however, we cannot make any strong claim at the moment. In all three EoS cases of hybrid mode, the minimum in slope is observed between 10A and 80A GeV. However, in the case of the bag model EoS, the minimum occurs near 10A–25A GeV while for case of other two EoS, the minimum is slightly shifted to higher energy and lies between 25A and

80A GeV. This shift in minimum leads to a splitting of slope parameters of $v_1(y)$ between the bag model and other two EoS which lie around 25A–30A GeV. A strong increase of slope in case of the bag model is observed which could possibly be a result of the inbuilt first-order phase transition, and perhaps hints towards the possible onset of deconfinement. In the past, a similar interesting feature around similar beam energy has been observed for the strange to nonstrange ratio [60]. Moreover, the slope of directed flow of protons is compared with the available experimental measurements of E895 [25], NA49 [58], and STAR [61] Collaborations as depicted in Fig. 3. It reveals that the results with hybrid mode overestimate the data beyond 2A GeV. Moreover, the slope of v_1 of pions and net protons is compared with STAR experiment measurements and it is observed that the inclusion of hydrodynamic expansion overestimates the measurements. According to the fluid dynamical calculations, the slope of v_1 of the baryons is expected to change sign, attributed to softening of EoS in the presence of a first-order phase transition. This was tested with various freeze-out scenarios using hydrodynamical simulations in Ref. [41]. On the other hand, the results with cascade mode underestimate the measurements below 6A GeV and
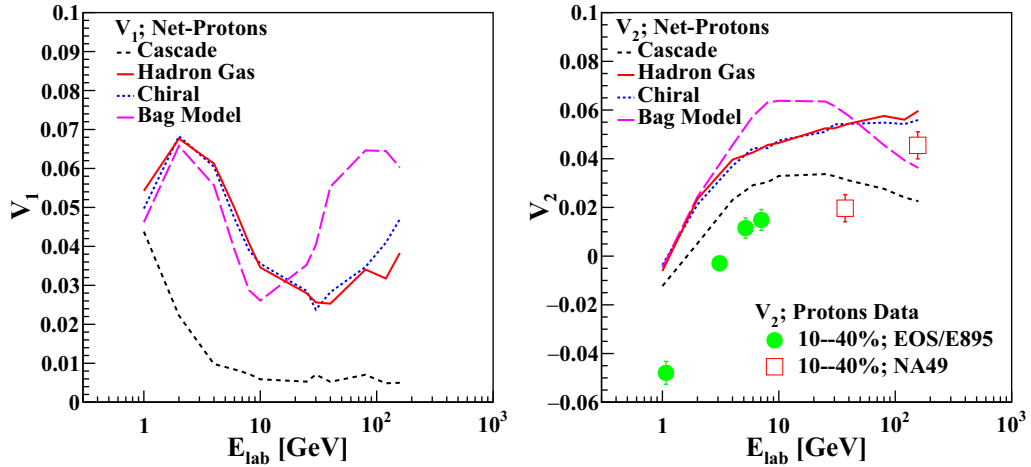
FIG. 4. p_T-integrated directed (v_1) (left) and elliptic (v_2) (right) flow of net protons as a function of beam energy at midrapidity ($0 < y_{c.m.} < 0.5$) for different configurations of UrQMD for noncentral ($b = 5$–9 fm corresponds to approximately 10-40% central) Au-Au collisions. In the right plot, v_2 of protons for $p_T < 2$ GeV/c is compared with available E895 and NA49 experimental measurements [21,58] in the investigated beam energy range in Au-Au and Pb-Pb collisions, respectively.

thereafter, showing a similar trend with slight overestimation above 30A GeV.

Moving forward, we attempt to look at the net protons for $p_T < 2$ GeV/c in more detail by inspecting their p_T-integrated directed and elliptic flow at midrapidity ($-0.5 < y_{c.m.} < 0.5$) as a function of beam energies, as shown in Fig. 4. In the left plot, we observe similar trends for v_1 as well its slope in all four cases studied here. Moreover, a feature of splitting at 20A–30A GeV in the presence of hydrodynamical evolution is also observed. In the case of v_2 in the right plot, we witness a similar splitting between the bag model EoS and the other two EoS. Furthermore, at beam energies around 10A–25A GeV a broad peak for v_2 in the case of the bag model can be seen and, for v_1 as well as its slope, there appear dips at similar beam energies. We repeat this exercise for v_2 of kaons and pions for $p_T < 2$ GeV/c as shown in Fig. 5, and here also kaons and

pions confirm the EoS dependent splitting in the hydro case; however, the splitting is not prominent in the case of pions. Furthermore, the v_2 of pions and net protons is also compared with the experimental measurements from E895 and NA49 Collaborations [21,58] and we saw overestimation of the data by hybrid mode here as well.

We now move our focus to look at the higher order flow harmonic coefficient v_4 which has been argued to be generated under the influence of fourth-order moment of fluid flow and the intrinsic elliptic flow, v_2 [34–36]. Under the assumption of ideal fluid dynamics and without any fluctuations, v_2 and v_4 are related to each other as $v_4 = 0.5(v_2)^2$. So one can expect to acquire some information about the transport properties of the nuclear fireball by estimating the ratio $v_4/(v_2)^2$. This ratio has been studied in our previous work [42] within beam energy range 6A–25A GeV for different equations of state
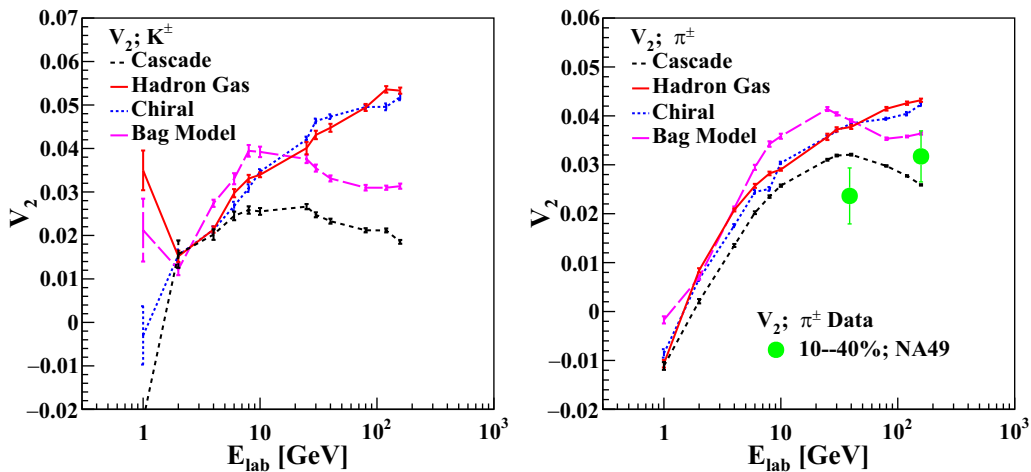

FIG. 5. p_T-integrated elliptic flow of kaons and pions as a function of beam energy at midrapidity ($-0.5 < y_{c.m.} < 0.5$) for different configurations of UrQMD for noncentral ($b = 5$–9 fm corresponds to approximately 10-40% central) Au-Au collisions. In the right plot, v_2 of pions for $p_T < 2$ GeV/c is compared with available NA49 experimental measurements [58] in the investigated beam energy range in Pb-Pb collisions.
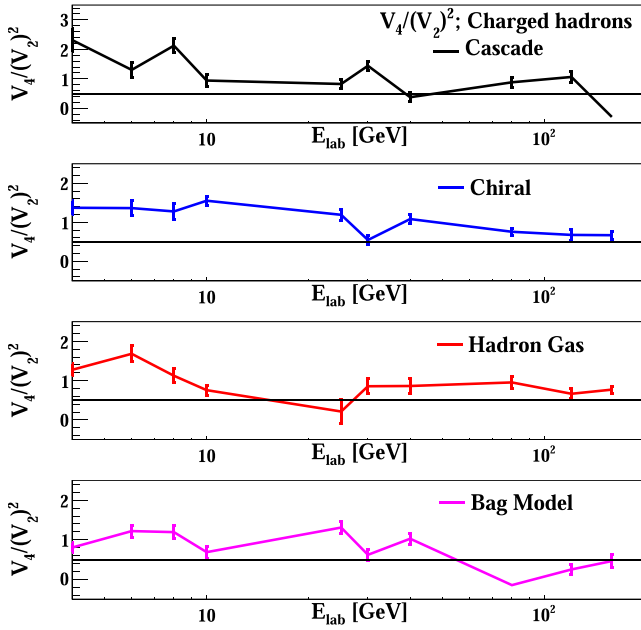
FIG. 6. $V_4/(V_2)^2$ of charged hadrons as a function of beam energy at midrapidity ($-0.5 < y_{c.m.} < 0.5$) for different configurations of UrQMD for noncentral ($b = 5-9$ fm corresponds to approximately 10-40% central) Au-Au collisions (E_{Lab} is given in GeV.). The horizontal line at 0.5 denotes the ideal fluid dynamic limit.

except the bag model. Prior to this, some phenomenological study was performed for this observable. In particular, observations using the parton-hadron string dynamics (PHSD) model [62] at different beam energies with Au-Au collisions have shown the ratio $v_4/(v_2)^2 \approx 2$. Moreover, the authors at Ref. [37] have attempted to investigate the enhancement of v_4 in low energy nuclear collisions using the JAM model. Experimentally, the results at RHIC [63–66] indicated the ratio to be unity. Figure 6 depicts the ratio as a function of beam energy (E_{Lab}) for different EoS, and the values always remain below 2 for all four cases. The ratio $v_4/(v_2)^2$ has been claimed to be associated with the phenomenon of incomplete equilibration in the literature [67]. However, the authors have studied this observable as a function of K^{-1}, the number of collisions per particle. Here K is the Knudsen number, a dimensionless quantity and a measure of degree of thermalization; it is a function of system size and beam energy. The local equilibration is expected to be reached when $K^{-1} \gg 1$. Moreover, the deviations from ideal hydrodynamics lead to incomplete thermal equilibrium. The ratio shown in Fig. 6 deviates from 0.5, giving the impression that the system is not fully equilibrated, thus preventing the use of ideal hydrodynamics in these beam energy regimes. The results here can be used to make some robust claims about the degree of thermalization of the nuclear fireball after comparison with the data available from future experiments at FAIR and NICA.

Last, we attempt to look at the number of constituent quark (NCQ) scaling in the flow coefficients for beam energies examined in this investigation. For this, we specially look at the slope of the directed flow of various species and their

combination under the assumption of the coalescence sum rule [68,69] for all four variants of UrQMD, and the results are shown in Fig. 7. First, similar to Ref. [68], we compare the dv_1/dy values of $\bar\Lambda$ $(\overline{uds})$ (black markers) with [K^- $(\bar us)$ $+ \frac{1}{3}\bar p$ $(\overline{uud})$] (red markers), where the same flow for s and $\bar s$ and, similarly, for $\bar u$ and $\bar d$ is assumed. The same kinematic coverages as in experimental measurements are applied in our simulations for all species. Our results are quantitatively higher than the ones presented in Ref. [68]; however, qualitatively, the sum rule seemed to be followed for these two cases at higher beam energies with slight hint of violation below 25A GeV, which at the moment cannot be strongly claimed due to large uncertainties in all four cases. For the same reason, we plot our results above 8A GeV up to 158A GeV. Moreover, we also look at one more set which is not as simple as earlier ones. As discussed in Ref. [68], different directed flows for transported[1] and produced[2] quarks are expected, and are not easy to distinguish in practice. The comparison of dv_1/dy of net Λ (uds) (blue triangular markers) with the calculation comprising different combinations of net p (uud), $\bar p$ $(\overline{uud})$, and K^- $(\bar us)$ (pink circle and blue square markers) is shown in Fig. 7. The combination of K^- and $\frac{1}{3}\bar p$ would give an s quark, which is assumed to replace the produced u quark in net p in the first coalescence calculation (pink circle markers). This calculation is expected to hold true at relatively higher energies where most of the quarks are produced and may not be valid at beam energies considered in this investigation, and this seems to be the case from our observations, as is evident from Fig. 7 for all four cases of UrQMD. In contrast, in the second calculation where net p is added up with the s quark, it is assumed that the transported quarks have dominant contribution in net p, which is quite suitable in the limit of low beam energies, and one of the quarks is replaced by an s quark. This calculation shows a nice agreement with net Λ between 25A and 158A GeV which then breaks down below 25A GeV in all four cases. This further may indicate towards possible confinement to deconfinement transition above 25A GeV which has been predicted in prior studies and also in our investigations earlier in this section. The results from our simulations are compared with the available experimental measurements from STAR Collaboration [68] and it is noticed that the measurements are overestimated. It is interesting to see the agreement of these sum rule calculations with EoS cases where the underlying degrees of freedom are not partonic, and this needs to be understood. However, the scaling behavior using the pure transport UrQMD model was also found earlier [13]. This also brings up the question of whether the underlying assumption of coalescence is indeed the source of this agreement. As mentioned earlier, the particle production in UrQMD at higher energies is performed in terms of string excitation and subsequent fragmentations as described in Refs. [17,70]. As per the string-excitation scheme, the quark-antiquark or diquark-antidiquark pairs are spontaneously formed in the color flux

---

[1]Quarks transported from the initial nuclei.
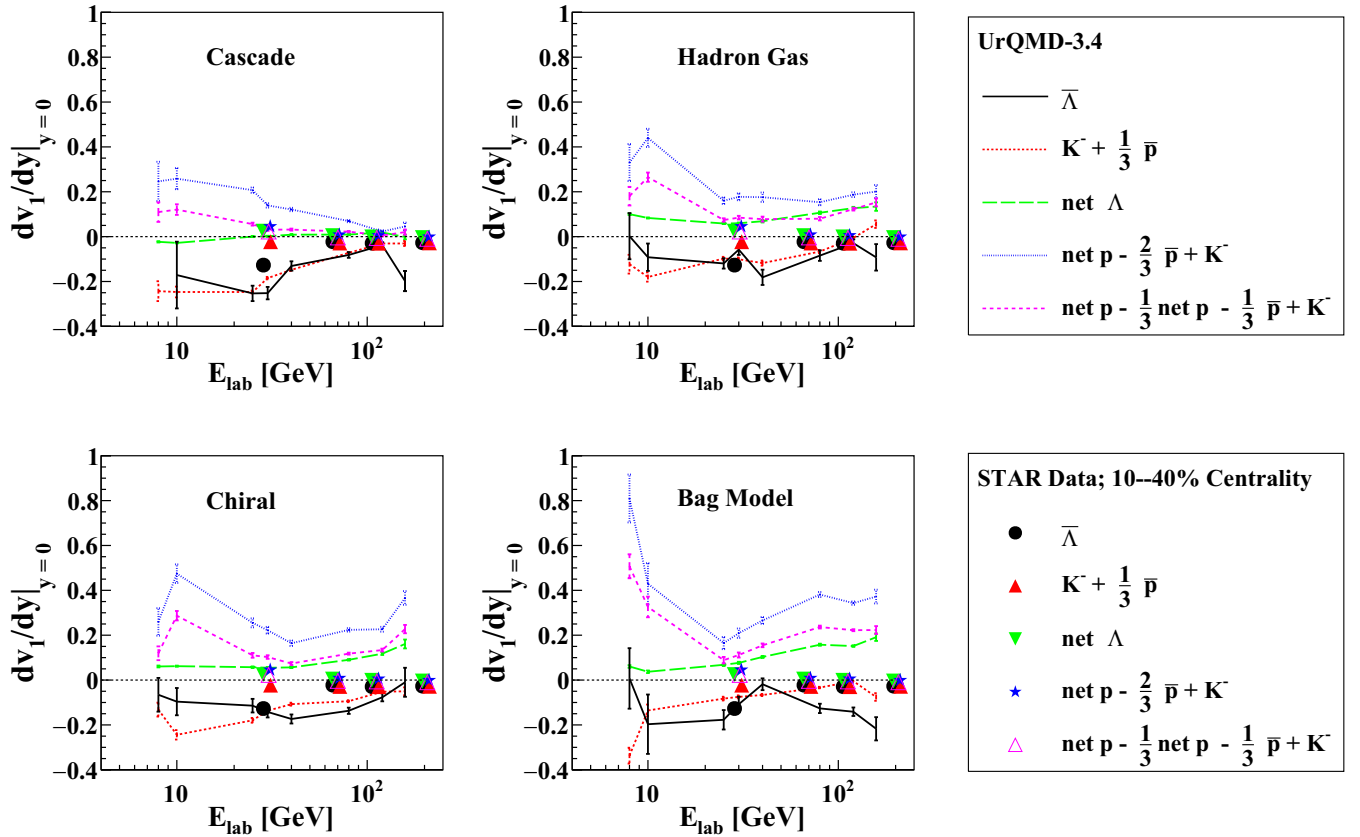
[2]Produced in the interactions.

FIG. 7. Comparison of slope of directed flow of net lambdas and antilambdas with various combinations of hadrons under the assumption of the coalescence sum rule as a function of beam energies for different configurations of UrQMD for noncentral ($b = 5$–9 fm corresponds to approximately 10-40% central) Au-Au collisions. Results from all variants are compared with STAR experimental measurements [68] in 10-40% central Au-Au collisions. Similar kinematic coverages as in data [68] are applied to the simulations.

tube between initial quarks, and subsequently mesons and baryons are produced. The produced hadrons undergo multiple scatterings; however, no string will be involved after a certain energy limit ($\sqrt{s} < 5$ GeV). This mechanism could give outcomes such as those shown in Fig. 7. It is also worthwhile to note that the additive quark model (AQM) is implemented in UrQMD to estimate the unknown hadronic cross sections [17]. This model assumes the existence of very weakly interacting dressed valence quarks inside the hadrons.

B. Particle ratios

In this subsection, we proceed to investigate and understand the effect of different degrees of freedom and phase transitions on the yield of the final state particles. For this, we obtain various particle ratios, namely, strange to nonstrange and antiparticle to particle, and compare them with the available data. For central collisions, the K^+/π^+ ratio has been studied in literature as a unique measure of the onset of deconfinement [60]. It will be interesting to see the behavior of this observable in the case of noncentral collisions. We estimate various particle ratios to procure insights about the medium properties by studying the impact of different equa-

tions of state. In Fig. 8, we show ratios of K^-/π^-, K^+/π^+. and $(K^+ + K^-)/(\pi^+ + \pi^-)$ as a function of beam energy for different cases of EoS. In the left plot, K^-/π^- shows a monotonic rise for all beam energies except for the bag model EoS which saturates after $20A$ GeV. In the middle plot, the K^+/π^+ ratio shows a similar increasing behavior up to $4A$ GeV and then starts to decrease with hint of stronger drop in the case of the bag model EoS between $20A$ and $30A$ GeV. In the rightmost plot, $(K^+ + K^-)/(\pi^+ + \pi^-)$ is obtained as a function of beam energy, and similar splitting, seen earlier between $20A$ and $30A$ GeV in the presence of a first-order phase transition, is observed. The ratio seems to saturate beyond this range in all other scenarios. Due to the unavailability of measurements in the desired centrality class, both K^-/π^- and K^+/π^+ ratios are compared with the experimental data from NA49 [73] and STAR experiments [74] at three different centralities, as these seem to cover impact parameters considered in this work. To demonstrate the centrality and beam energy dependence, we also compare our predictions of various particle ratios with measurements at most central as well as peripheral collisions. From Fig. 8, it can be seen that the chiral and hadron gas EoS are able to reproduce the trend set by data in both these ratios; however, the magnitude is overestimated. Furthermore, we also look at the antiparticle to particle ratio for different
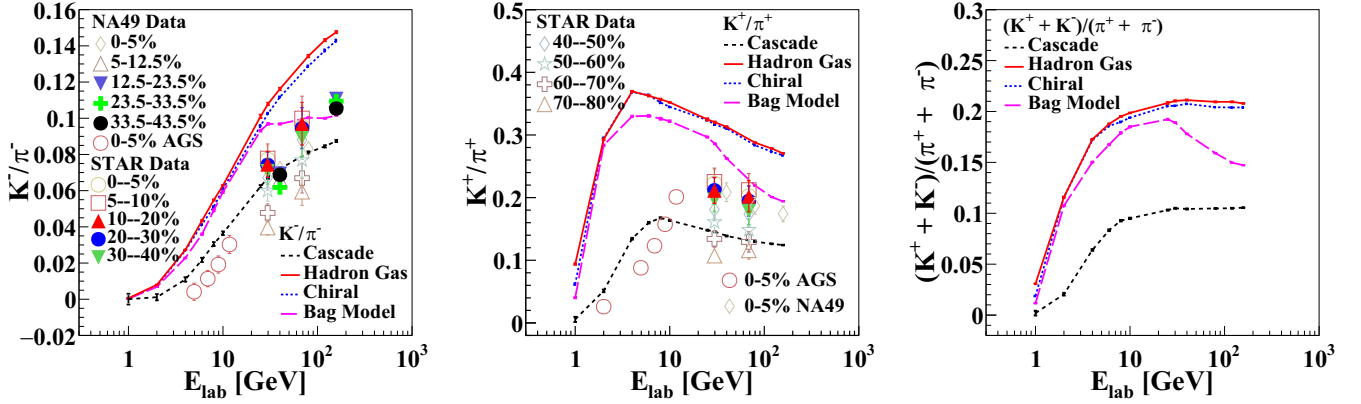
FIG. 8. K^- to π^-, K^+ to π^+, and $(K^+ + K^-)/(\pi^+ + \pi^-)$ ratios as a function of beam energy for different configurations of UrQMD for noncentral ($b = 5$–9 fm corresponds to approximately 10-40% central) Au-Au collisions and their comparison with AGS [71], NA49 [72,73], and STAR experimental measurements [74] in Au-Au, Pb-Pb, and Au-Au collisions for all available centralities, respectively. Vertical bars on the data denote statistical uncertainties.

EoS. In Fig. 9, K^+/K^-, π^+/π^-, and $\bar{p}/p$ ratios are depicted for all four cases of fireball evolution. The K^+/K^- ratio shows an increase for all beam energies and EoS; however, no sensitivity to a specific EoS is detected. In the middle plot of Fig. 9, we see the same magnitude of π^+/π^- ratio for all EoS at all energies beyond $4A$ GeV, with decreasing trend as a function of beam energy. Moreover, data seem to favor hybrid mode for both ratios, with slight underestimation by hybrid in the case of the K^+/K^- ratio. The antiproton to proton ratio is shown in the rightmost plot and compared with experimental data. Measurements are relatively underestimated by the model in all cases of EoS. Finally, we study the p/π^+ and $\bar{p}/\pi^-$ ratios and compare them with the available data as shown in Fig. 10. In the former case, the ratio is inversely proportional to beam energy and shows similar magnitude for all hybrid cases, with slightly higher magnitude in the cascade case at all beam energies. The ratio using hybrid mode shows good agreement with the experimental measurement, as depicted in the left plot. In the right plot of Fig. 10, the $\bar{p}/\pi^-$ ratio shows a trend similar to data, and sensitivity to first-order

phase transition. The reader may take note of the fact that for protons the comparison of the UrQMD model calculations with the experimentally measured data are to be accepted with a caveat. In low energy collisions ($E_{\mathrm{Lab}} \lesssim 10A$ GeV) the production of light nuclei (d, t, He) has a non-negligible contribution. The model calculates the so-called primordial nucleons, which still contain the contribution of the nucleons bound in the light nuclei. This concerns all observables involving protons. However, for anisotropic flow coefficients the effect of bound the proton is considerably reduced because of their independence of proton multiplicity. But it is important for the observables like particle ratios presented in Figs. 9 and 10 involving proton yield, as well net-proton rapidity distribution shown in Fig. 11 (next subsection). A consistent way to take the light nuclei into account is by coalescing the final state nucleons from UrQMD. The basic philosophy behind the coalescence approach is to check for clusters of nucleons at freeze-out with a very small momentum difference that happen to be very close to each other. However, this is beyond the scope of the present work.
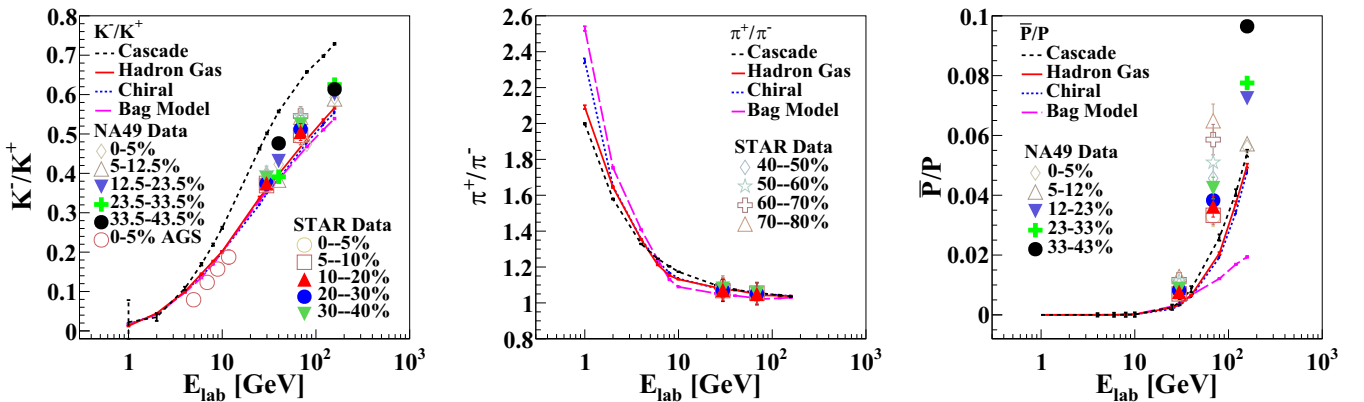

FIG. 9. K^- to K^+, π^+ to π^-, and antiproton to proton ratios as a function of beam energy for different configurations of UrQMD for noncentral ($b = 5$–9 fm corresponds to approximately 10-40% central) Au-Au collisions and their comparison with AGS [75], NA49 [73], and STAR experimental measurements [74] in Au-Au, Pb-Pb, and Au-Au collisions for all available centralities, respectively. Vertical bars on the data denote statistical uncertainties.
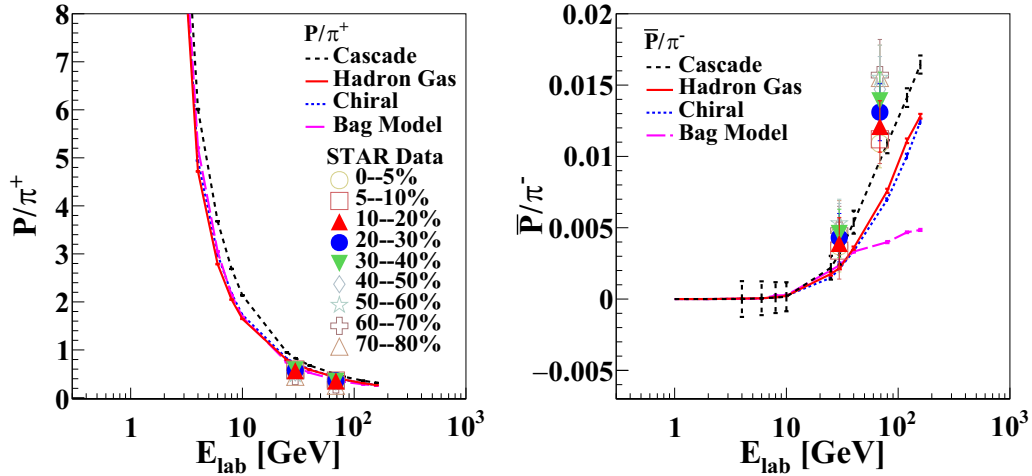
FIG. 10. Proton to π^+ and antiproton to π^- ratios as a function of beam energy for different configurations of UrQMD for noncentral ($b = 5$–9 fm corresponds to approximately 10-40% central) Au-Au collisions and their comparison with STAR experimental measurements [74] in Au-Au collisions for all available centralities. Vertical bars on the data denote statistical uncertainties.
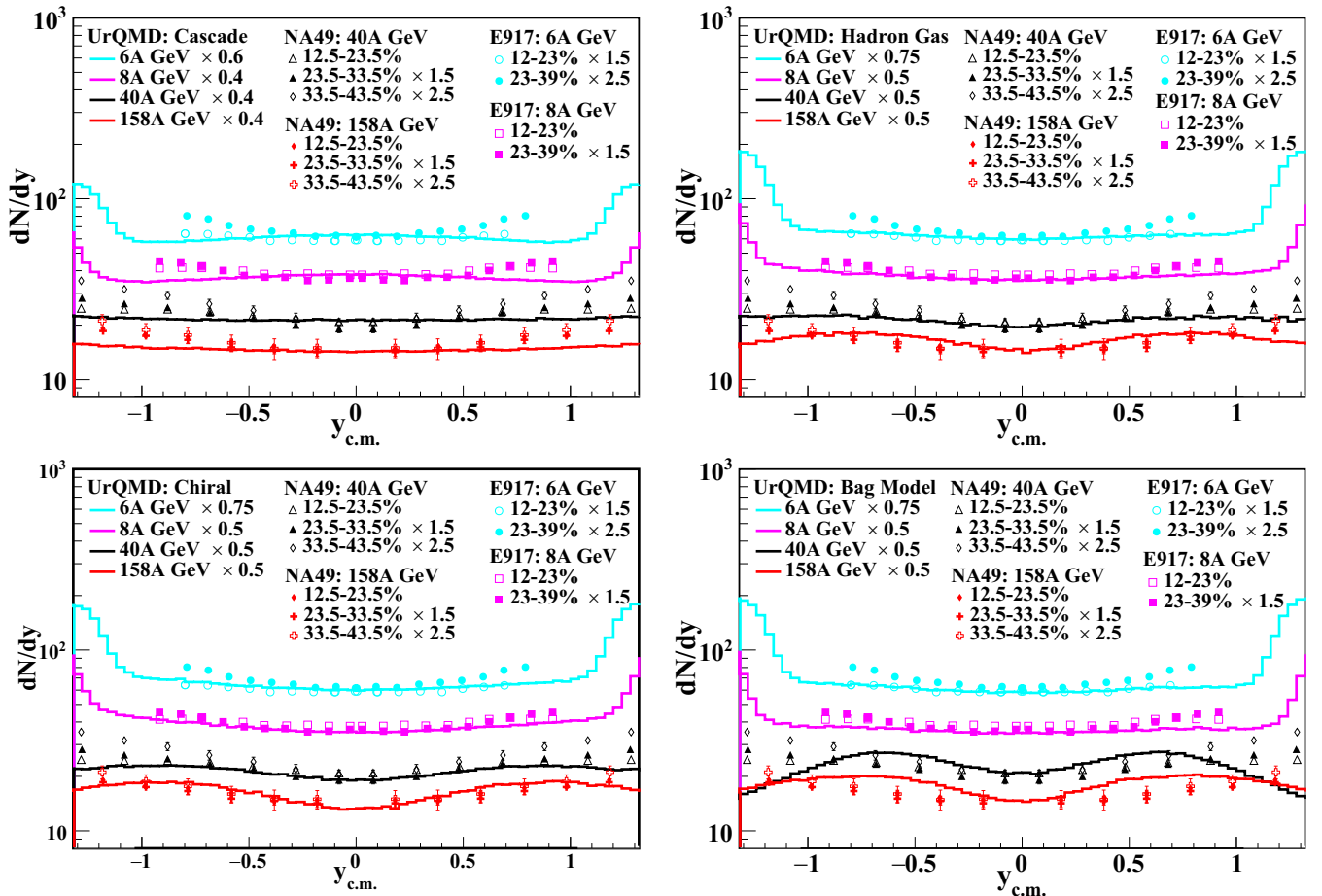

FIG. 11. Rapidity spectra of net protons at various beam energies for different equations of state for noncentral ($b = 5$–9 fm corresponds to approximately 10-40% central) Au-Au collisions and their comparison with the measured rapidity spectra of net protons in Au-Au and Pb-Pb collisions by E917 [76] and NA49 [77] Collaborations, respectively. Both simulation results and measurements are scaled for better visualization. Vertical bars on the data denote statistical uncertainties.

C. Net-proton rapidity spectra

Understanding the in-medium properties of stopped protons by studying their rapidity distributions has been a promising observable. In Refs. [43–47], multiple studies in this direction have been performed. It has been argued that the irregularities in the distribution of stopped protons may well be the consequence of onset of a deconfinement transition. This occurs due to the inherited softest point in the nuclear equations of state in the vicinity of a phase transition. Such investigations are generally performed in central collisions; however, it is also worthwhile to check this in noncentral collisions as well. The shape of rapidity spectra at midrapidity may contain very crucial information about the medium and is believed to be sensitive to the underlying nuclear equations of state. Therefore, we look at the net-proton rapidity distribution at different beam energies and equations of state. In Fig. 11, we show rapidity distribution of net protons at midrapidity for all energies and EoS considered in this work. Rapidity spectra remain flat at high beam energies in case of cascade mode, in contrast to hybrid mode where they show a very interesting feature. These results are compared with the measured rapidity spectra at available energies from E917 [76] and NA49 [77] experiments in the centrality regions covering the investigated range. Our results overestimate the measurements at all available beam energies.

As the irregularities in the shape of rapidity spectra at midrapidity can potentially help in explaining the dynamics of the medium, we quantify the nature of simulated as well as the measured spectra at midrapidity by calculating the double derivative of the rapidity spectra at midrapidity, i.e., global minima or maxima as shown in Fig. 12. This quantity is identical to the one obtained in the Refs. [43–47] and is referred to as reduced curvature. For this, the rapidity distributions of net protons are fitted with polynomials at midrapidity for all beam energies and EoS. As shown in Fig. 12, the reduced curvature in the case of cascade remains constant and zero for all energies. As soon as the hydrodynamical evolution is introduced, the corresponding observable shows some sensitivity as a function of beam energy. Similarly to simulations, the reduced curvatures of measured rapidity spectra shown in Fig. 11 are calculated, and it is seen that they remain almost flat; however, they are slightly higher than in the cascade case at all beam energies. They almost match the hybrid scenario at 6*A*, 8*A*, and 40*A* GeV and are slightly lower in the hybrid mode case at 158*A* GeV. We do not notice the so-called "peak-dip-peak-dip" irregularity as seen in the experimental observations and in central collisions [43–47]. It may also be mentioned that in Ref. [43–47], the contribution of nucleons bound in the light nuclei was subtracted from primordial nucleons by means of coalescence, whereas our results still suffer from the uncertainty due to inclusion of the contribution from bound protons, as detailed earlier. Still, it is interesting to note that this observable has led to show the sensitivity between chiral and hadron gas EoS beyond 25*A* GeV, which is the same energy at which we have seen some interesting features for other observables investigated in this work. The magnitude and slope of reduced curvature is highest for the bag model and decreases for chiral and hadron gas beyond
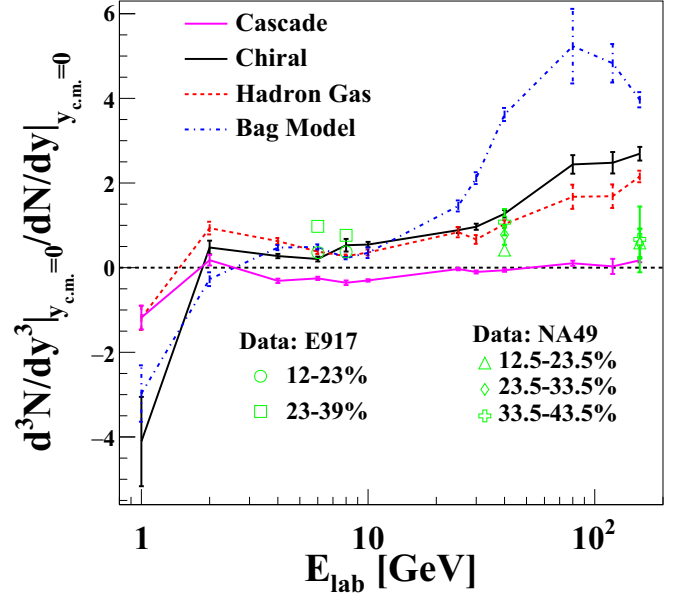

FIG. 12. Reduced curvature of rapidity spectra of net protons as a function of beam energy for different configurations of UrQMD for noncentral ($b = 5$–9 fm corresponds to approximately 10-40% central) Au-Au collisions at midrapidity ($-0.5 < y_{c.m.} < 0.5$) and its comparison with the calculated reduced curvature of measured rapidity spectra of net protons in noncentral Au-Au and Pb-Pb collisions by E917 [76] and NA49 [77] Collaborations, respectively.

25*A* GeV. In the end, it is worth mentioning that the net protons are the only species for which any sensitivity to the underlying degrees of freedom has been noticed, especially for the observables related to longitudinal dynamics such as directed flow and rapidity.

IV. SUMMARY

In this article, we have made dedicated efforts to understand the impact of various nuclear equations of state on several observables of the nuclear matter produced in low energy collisions of heavy ions in a wide range of beam energies, 1*A*-158*A* GeV. The UrQMD model with intermediate hydrodynamical evolution was employed with different nuclear equations of state such as hadron gas, chiral + deconfinement, and the bag model. We started with examining the anisotropic flow coefficients of charged and identified hadrons in the above-mentioned beam energy range. A unique feature at 25*A*–30*A* GeV in the energy dependence of slopes of directed flow of charged hadrons, protons, and netprotons at midrapidity was observed. The slope using the bag model EoS showed a splitting, leading to a sharp rise compared to the other two equations of state. This may be attributed to the incorporated first-order phase transition in the former case. A similar feature was observed for directed flow as well. Apart from the splitting, the dip within a certain energy range for these equations of state hints towards possible onset of deconfinement. Moreover, we noticed that study of net-proton rapidity distribution certainly brings out the sensitivity to underlying degrees of freedom in chiral and hadron gas EoS

beyond $20A$–$30A$ GeV beam energy; however, more evidence in this direction is required to make any robust claim. Along with this, efforts have been made to study the effect of different EoS on elliptic flow (v_2) of identified hadrons as a function of the beam energy (E_{Lab}). As quadrangular flow, v_4, is believed to originate from v_2 and fourth-order moment of the fluid flow, the ratio $v_4/(v_2)^2$ was examined for wide range of beam energies and different EoS. The ratio is always found to be below 2 for all four cases of EoS and can be tested against the data from the future experiments at NICA [8] and FAIR [9,10].

In addition, we have studied NCQ scaling in terms of the coalescence sum rule for slope of directed flow of $\bar{\Lambda}$ and net Λ. For this purpose, we used different calculations than used in Ref. [68] and compared them with dv_1/dy of $\bar{\Lambda}$ and net Λ. Results qualitatively match the expectations for all four variants of UrQMD. This study may also hint towards possible onset of deconfinement at a certain beam energy above $25A$ GeV. Furthermore, it was interesting to notice similar nature of the results even for pure transport and hadrons gas EoS cases where quarks and gluons are not underlying degrees of freedom.

At this point, it appears from the results of collective flow excitation functions that neither of the EoS is suitable enough to quantitatively reproduce the experimental measurements. Moreover, the nature of the matter might be partonic; however, it does not evolve as a nonviscous ideal fluid as implemented in the present version of the model. Furthermore, higher values of calculated flow coefficients corresponding to data suggest larger pressure gradient in the ideal hydrodynamic scenario and, therefore, one possibility would be to use viscous hydrodynamics instead of ideal to account for dissipative effects. Other reasons for the disagreement might be inapplicability of hydrodynamics at low beam energies, where the transport approach seems to give better agreement, and also

the fact that reaction plane angles which lead to event by event fluctuations are not taken into account in UrQMD.

Various particle ratios are calculated for all EoS and studied as a function of beam energy. The ratios were found to be sensitive to first-order phase transition and exhibited different behavior in comparison to other cases. UrQMD including fluid dynamic simulations with hadron gas and chiral EoS is qualitatively able to explain the measured strange to nonstrange ratio and overestimate the measurements. However, the calculated strange to nonstrange ratio showed some interesting features in response to various EoS beyond $25A$ GeV. Similarly, particle to antiparticle ratios are qualitatively described by hybrid mode with underestimation with respect to the data, except for the π^+/π^- ratio which is nicely explained. Moreover, the measured ratio of proton to π^+ is also well described by the predictions; however, the calculated antiproton to π^- ratio underestimates the data.

We wrap up by studying the rapidity spectra of net protons for different EoS at various beam energies. The shape of these spectra at midrapidity, quantified as a reduced curvature, is seen to be sensitive to underlying EoS and shows a larger value in the case of bag model EoS beyond $25A$ GeV. It also revealed the sensitivity to the underlying degrees of freedom beyond $25A$ GeV. These investigations provide an opportunity to understand the behavior of various observables under different nuclear equations of state and to compare the results with the outcomes from future experiments.

ACKNOWLEDGMENTS

[1] W. Florkowski, Acta Phys. Pol. B **45**, 2329 (2014).

[2] P. Braun-Munzinger and J. Wambach, Rev. Mod. Phys. **81**, 1031 (2009).

[3] J. Adams *et al.* (STAR Collaboration), Nucl. Phys. A **757**, 102 (2005).

[4] K. Adcox *et al.* (PHENIX Collaboration), Nucl. Phys. A **757**, 184 (2005).

[5] K. Aamodt *et al.* (ALICE Collaboration), Phys. Rev. Lett. **107**, 032301 (2011).

[6] G. Aad *et al.* (ATLAS Collaboration), Phys. Rev. C **86**, 014907 (2012).

[7] S. Chatrchyan *et al.* (CMS Collaboration), Phys. Rev. C **89**, 044906 (2014).

[8] V. Kekelidze, A. Kovalenko, R. Lednicky, V. Matveev, I. Meshkov, A. Sorin, and G. Trubnikov, Nucl. Phys. A **956**, 846 (2016).

[9] T. Ablyazimov *et al.* (CBM Collaboration), Eur. Phys. J. A **53**, 60 (2017).

[10] C. Sturm, B. Sharkov, and H. Stöcker, Nucl. Phys. A **834**, 682c (2010).

[11] B. Alver *et al.* (PHOBOS Collaboration), Phys. Rev. Lett. **98**, 242302 (2007).

[12] K. Aamodt *et al.* (ALICE Collaboration), Phys. Rev. Lett. **105**, 252302 (2010).

[13] P. P. Bhaduri and S. Chattopadhyay, Phys. Rev. C **81**, 034906 (2010).

[14] S. Sarkar, P. Mali, and A. Mukhopadhyay, Phys. Rev. C **95**, 014908 (2017).

[15] J. Auvinen and H. Petersen, Phys. Rev. C **88**, 064908 (2013).

[16] S. A. Bass, M. Belkacem, M. Bleicher, M. Brandstetter, L. Bravina, C. Ernst, L. Gerland, M. Hofmann, S. Hofmann, J. Konopka *et al.*, Prog. Part. Nucl. Phys. **41**, 255 (1998).

[17] M. Bleicher, E. Zabrodin, C. Spieles, S. A. Bass, C. Ernst, S. Soff, L. Bravina, M. Belkacem, H. Weber, H. Stoecker *et al.*, J. Phys. G **25**, 1859 (1999).

[18] Z. W. Lin, C. M. Ko, B. A. Li, B. Zhang, and S. Pal, Phys. Rev. C **72**, 064901 (2005).

[19] L. W. Chen, V. Greco, C. M. Ko, and P. F. Kolb, Phys. Lett. B **605**, 95 (2005).

[20] A. Le Fèvre, Y. Leifels, C. Hartnack, and J. Aichelin, Phys. Rev. C **98**, 034901 (2018).

[21] C. Pinkenburg *et al.* (E895 Collaboration), Phys. Rev. Lett. **83**, 1295 (1999).

[22] Y. Nara, H. Niemi, A. Ohnishi, and H. Stöcker, Phys. Rev. C **94**, 034906 (2016).

[23] Y. Nara, N. Otuka, A. Ohnishi, K. Niita, and S. Chiba, Phys. Rev. C **61**, 024901 (1999).

[24] V. P. Konchakovski, W. Cassing, Y. B. Ivanov, and V. D. Toneev, Phys. Rev. C **90**, 014903 (2014).

[25] H. Liu *et al.* (E895 Collaboration), Phys. Rev. Lett. **84**, 5488 (2000).

[26] P. Chung *et al.* (E895 Collaboration), Phys. Rev. Lett. **85**, 940 (2000).

[27] P. Chung, N. N. Ajitanand, J. M. Alexander, M. Anderson, D. Best, F. P. Brady, T. Case, W. Caskey, D. A. Cebra, J. L. Chance *et al.*, Phys. Rev. Lett. **86**, 2533 (2001).

[28] H. Appelshauser *et al.* (NA49 Collaboration), Phys. Rev. Lett. **80**, 4136 (1998).

[29] J. Adams *et al.* (STAR Collaboration), Phys. Rev. C **72**, 014904 (2005).

[30] B. B. Back *et al.* (PHOBOS Collaboration), Phys. Rev. Lett. **97**, 012301 (2006).

[31] R. J. M. Snellings, H. Sorge, S. A. Voloshin, F. Q. Wang, and N. Xu, Phys. Rev. Lett. **84**, 2803 (2000).

[32] L. P. Csernai and D. Rohrich, Phys. Lett. B **458**, 454 (1999).

[33] J. Brachmann, S. Soff, A. Dumitru, H. Stöcker, J. A. Maruhn, W. Greiner, L. V. Bravina, and D. H. Rischke, Phys. Rev. C **61**, 024909 (2000).

[34] N. Borghini and J. Y. Ollitrault, Phys. Lett. B **642**, 227 (2006).

[35] C. Gombeaud and J. Y. Ollitrault, Phys. Rev. C **81**, 014901 (2010).

[36] M. Luzum, C. Gombeaud, and J. Y. Ollitrault, Phys. Rev. C **81**, 054910 (2010).

[37] Y. Nara, J. Steinheimer, and H. Stoecker, Eur. Phys. J. A **54**, 188 (2018).

[38] A. Adare *et al.* (PHENIX Collaboration), Phys. Rev. C **93**, 024901 (2016).

[39] H. Petersen, Q. Li, X. Zhu, and M. Bleicher, Phys. Rev. C **74**, 064908 (2006).

[40] H. Petersen and M. Bleicher, Phys. Rev. C **79**, 054904 (2009).

[41] J. Steinheimer, J. Auvinen, H. Petersen, M. Bleicher, and H. Stöcker, Phys. Rev. C **89**, 054913 (2014).

[42] S. P. Rode, P. P. Bhaduri, and A. Roy, Eur. Phys. J. A **55**, 216 (2019).

[43] Y. B. Ivanov, Phys. Lett. B **690**, 358 (2010).

[44] Y. B. Ivanov, Phys. Lett. B **721**, 123 (2013).

[45] Y. B. Ivanov, Phys. Lett. B **723**, 475 (2013).

[46] Y. B. Ivanov and D. Blaschke, Phys. Rev. C **92**, 024916 (2015).

[47] Y. B. Ivanov and D. Blaschke, Eur. Phys. J. A **52**, 237 (2016).

[48] H. Petersen, J. Steinheimer, G. Burau, M. Bleicher, and H. Stöcker, Phys. Rev. C **78**, 044901 (2008).

[49] D. H. Rischke, S. Bernard, and J. A. Maruhn, Nucl. Phys. A **595**, 346 (1995).

[50] D. H. Rischke, Y. Pursun, and J. A. Maruhn, Nucl. Phys. A **595**, 383 (1995); **596**, 717(E) (1996).

[51] F. Cooper and G. Frye, Phys. Rev. D **10**, 186 (1974).

[52] E. Santini, B. Bauchle, H. Petersen, J. Steinheimer, M. Nahrgang, and M. Bleicher, Nuovo Cimento C **34N2**, 119 (2011).

[53] J. Steinheimer, V. Dexheimer, M. Bleicher, H. Petersen, S. Schramm, and H. Stöcker, Phys. Rev. C **81**, 044913 (2010).

[54] H. Petersen, J. Steinheimer, M. Bleicher, and H. Stocker, J. Phys. G **36**, 055104 (2009).

[55] D. Zschiesche, S. Schramm, J. Schaffner-Bielich, H. Stoecker, and W. Greiner, Phys. Lett. B **547**, 7 (2002).

[56] A. Chodos, R. L. Jaffe, K. Johnson, C. B. Thorn, and V. F. Weisskopf, Phys. Rev. D **9**, 3471 (1974).

[57] J. Steinheimer, S. Schramm, and H. Stocker, Phys. Rev. C **84**, 045208 (2011).

[58] C. Alt *et al.* (NA49 Collaboration), Phys. Rev. C **68**, 034903 (2003).

[59] H. Stocker, PoS **CPOD07**, 025 (2007).

[60] C. Alt *et al.* (NA49 Collaboration), Phys. Rev. C **77**, 024903 (2008).

[61] L. Adamczyk *et al.* (STAR Collaboration), Phys. Rev. Lett. **112**, 162301 (2014).

[62] V. P. Konchakovski, E. L. Bratkovskaya, W. Cassing, V. D. Toneev, S. A. Voloshin, and V. Voronyuk, Phys. Rev. C **85**, 044922 (2012).

[63] J. Adams *et al.* (STAR Collaboration), Phys. Rev. Lett. **92**, 062301 (2004).

[64] H. Masui *et al.* (PHENIX Collaboration), Nucl. Phys. A **774**, 511 (2006).

[65] B. I. Abelev *et al.* (STAR Collaboration), Phys. Rev. C **75**, 054906 (2007).

[66] S. Huang *et al.* (PHENIX Collaboration), J. Phys. G **35**, 104105 (2008).

[67] R. S. Bhalerao, J. P. Blaizot, N. Borghini, and J. Y. Ollitrault, Phys. Lett. B **627**, 49 (2005).

[68] L. Adamczyk *et al.* (STAR Collaboration), Phys. Rev. Lett. **120**, 062301 (2018).

[69] J. C. Dunlop, M. A. Lisa, and P. Sorensen, Phys. Rev. C **84**, 044914 (2011).

[70] Y. Guo, F. Liu, and A. Tang, Phys. Rev. C **86**, 044901 (2012).

[71] L. Ahle *et al.* (E866 and E917 Collaboration), Phys. Lett. B **476**, 1 (2000).

[72] S. V. Afanasiev *et al.* (NA49 Collaboration), Phys. Rev. C **66**, 054902 (2002).

[73] C. Alt *et al.* (NA49 Collaboration), Phys. Rev. C **73**, 044910 (2006).

[74] L. Adamczyk *et al.* (STAR Collaboration), Phys. Rev. C **96**, 044904 (2017).

[75] L. Ahle *et al.* (E866 and E917 Collaboration), Phys. Lett. B **490**, 53 (2000).

[76] B. B. Back *et al.* (E917 Collaboration), Phys. Rev. Lett. **86**, 1970 (2001).

[77] T. Anticic *et al.* (NA49 Collaboration), Phys. Rev. C **83**, 014901 (2011).